Evaluation of Gunshot Detection Algorithms

Alfonso Chacón-Rodríguez, *Member, IEEE*, Pedro Julián, *Senior Member, IEEE*, Liliana Castro, Pablo Alvarado, *Member, IEEE*, and Néstor Hernández

***Abstract*—Six preprocessing algorithms for the detection of firearm gunshots are statistically evaluated, using the receiver operating characteristic method as a previous feasibility metric for their implementation on a low-power VLSI circuit. Circuits are intended to serve as the input detection sensors of a low-power environmental surveillance network. Some possible VLSI implementations for the evaluated algorithms are also evaluated. Results indicate that the use of wavelet bank filters, either discrete or continuous, might be the best choice in terms of the compromise between detection efficiency and the power requirements of the intended application.**

***Index Terms*—Gunshot detection, low-power VLSI, mixed-signal application-specified integrated circuit, signal processing.**

I. Introduction

DETECTION, classification, and localization of gunshots are of particular interest in areas related to public health, surveillance, law enforcement, and the military. There is plenty of research regarding gunshot theory and the needs for its study (see [1]–[4]), as well as many software and hardware implementations of computationally efficient signal processing analysis methods [5]–[11]. These solutions mostly use complex algorithms, such as short-time Fourier transform, wavelet transforms, hidden Markov models, Gaussian mixtures, and maximum likelihood models, and claim to be very effective at detecting, classifying, and localizing shots from different firearms. Yet, such algorithms are expensive in terms of power due to their computational needs, which range from the whole personal computer systems to mote-oriented sensor networks with DSP-dedicated chips and embedded processors, making their deployment on the field cumbersome mainly because of their energy requirements. One particular instance of interest is the establishment of a surveillance network against illegal hunting in tropical forest reserves. In such environment, low-power sensor networks provide a feasible solution, considering the large areas to be protected and the near impossibility of providing the sensors with standard long-lasting power supplies. Although there are some commercial solutions available in that area (see [9] and [12]), all of them entail the use of equipment and algorithms that claim to be efficient in terms of processing but not in terms of power dissipation, questioning the use of complex classification methods at least in the early stages of detection.

Regarding the complexities behind gunshot and firearm detection and classification, Maher offers a very thorough explanation of the physics of a gunshot in [1] and [2]. Gunshot sound is produced by two phenomena: first, the muzzle blast, which is produced by the rapidly expanding gases from the confined explosive charge that is used to propel the bullet out of the gun barrel. This acoustic disturbance lasts 3–5 ms and propagates through the air at the speed of sound. Second, if the bullet travels at supersonic speed, it causes an acoustic shock wave that propagates away from the bullet's path. The shock wave expands as a cone behind the bullet, with the wave front propagating outward at the speed of sound.

A typical gunshot signature is shown in Fig. 1. The sound characteristics of any gunshot are thus determined by factors such as the caliber of the bullet and the barrel, the length of the latter, and the chemical properties of the propellant. Moreover, being a nearly perfect impulsive signal, any particular measurement of the spectral or impulsive characteristics of a particular gunshot will likely give more information about the acoustic surroundings (i.e., the surrounding's acoustic impulse response) rather than the firearm's or the projectile's characteristics [1], [2], which, in turn, are dependent on a multiple set of factors such as temperature, wind speed, foliage density, air moisture, and soil characteristics [13]. Attempts at detecting the N-shaped shock wave (as Sadler *et al.* report using a wavelet approach [7]) become difficult as the wave rapidly loses its shape due to nonlinear dispersion or disappears altogether once the bullet's speed falls under supersonic speed or hits an obstacle, a possibility which is higher in such a dense setting as a tropical rain forest. On the other hand, looking at the power spectra of three particular gunshots gives also an idea of the differences between firearms located at the same distance (Fig. 2), which simply discourages the use of a simple filtering method for the task of detection.

Considering all these, a solution is proposed, where a signal detector would be used as an initial low-power processing stage in each node of the surveillance network. In the case of a gunshot, this detector would activate a subsequent classification stage in that same node, which would either process the signal

Manuscript received December 29, 2009; revised May 17, 2010 and July 12, 2010; accepted July 17, 2010. Date of publication November 09, 2010; date of current version January 28, 2011. This work was supported in part by the Consejo Nacional de Investigaciones Científicas y Técnicas under Projects ANPCyT-PICT 2006 1835, PGI-UNS 2006 24/ZK17, and PIP 2005–2006 5048 and in part by ANPCyT-PAE 37079, Argentina. The work of A. Chacón-Rodríguez was supported in part by the Instituto Tecnológico de Costa Rica, by the Ministerio de Ciencia y Tecnología, and by the Consejo Nacional de Investigaciones Científicas y Tecnológicas de Costa Rica. This paper was recommended by Associate Editor H. Schmid.

A. Chacón-Rodríguez, P. Alvarado, and N. Hernández are with the Escuela de Ingeniería Electrónica, Instituto Tecnológico de Costa Rica, Cartago 30101, Costa Rica.

P. Julián is with the Instituto de Investigaciones en Ingeniería Eléctrica, Departamento de Ingeniería Eléctrica y de Computadoras, Consejo Nacional de Investigaciones Científicas y Técnicas/Universidad Nacional del Sur, Bahía Blanca B8000CPB, Argentina.

L. Castro is with the Instituto de Investigaciones en Ingeniería Eléctrica, Departamento de Ingeniería Eléctrica y de Computadoras, Consejo Nacional de Investigaciones Científicas y Técnicas/Universidad Nacional del Sur, Bahía Blanca B8000FTN, Argentina, and also with the Departamento de Matemática, Universidad Nacional del Sur, Bahía Blanca B8000CPB, Argentina.

Digital Object Identifier 10.1109/TCSI.2010.2072052

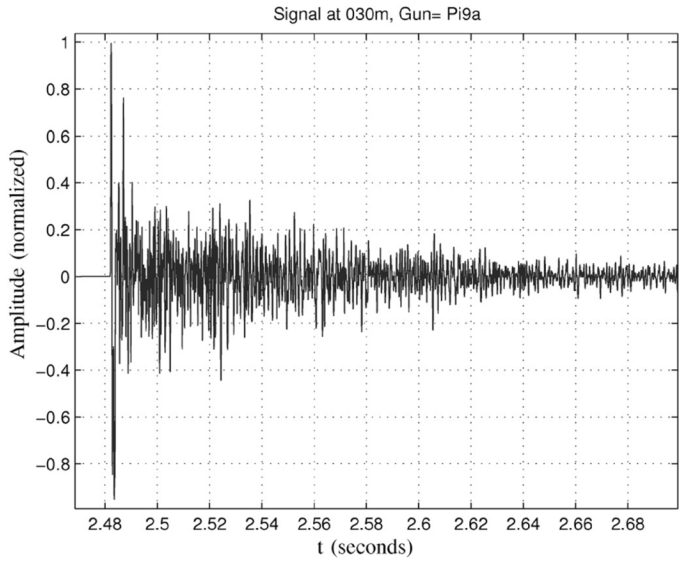

Fig. 1. Typical time signature of a gunshot: 9-mm pistol at 30-m range from the recording microphone. Multipath distortion is appreciated a few milliseconds after the first peak.

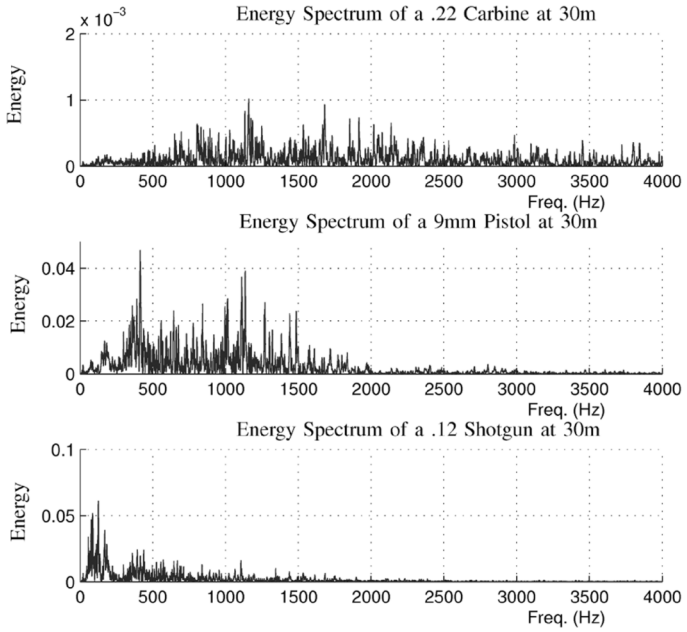

Fig. 2. Examples of the power spectra for a .22 carbine, a 9-mm pistol, and a .12 shotgun recorded at 30 m.

with an advanced (and, therefore, power hungry) algorithm or transmit the acquired data through the network for further processing. Thus, an evaluation of the efficiency of any detection algorithm and the feasibility of its low-power implementation becomes mandatory before proposing a particular solution for this initial stage. A previous report on five of the algorithms has been shown in [14]. A sixth algorithm is included here, some extra evaluations were done on two of the other algorithms, and additional considerations were taken regarding the alternatives for their physical realization. This paper is organized as follows: Section II depicts the typical basic detection architecture, Section III explains the six algorithms that were evaluated, Section IV shows the analysis of the results, and, finally, Section V presents the conclusions.

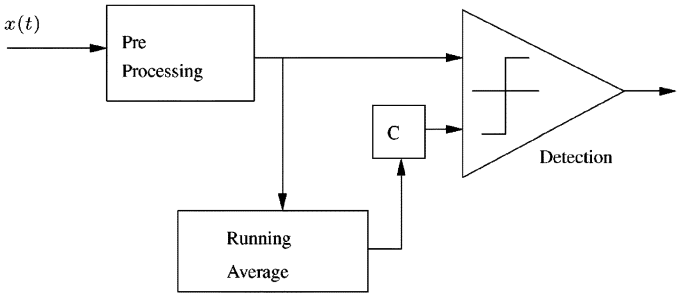

Fig. 3. Basic structure of the detection algorithm. The adaptive threshold is typically a running average or rms estimation of the preprocessed signal. C serves as a threshold gain that allows to fine tune the selectiveness of the detection.

II. Basic Detection Architecture and ROC Specifications

The proposed detection scheme is shown in Fig. 3 and is common in the field of biomedical engineering for the detection of neural spikes [15] and also in other applications involving detection and classification of impulsive audio events [5]. Detection is achieved by the comparison between a preprocessed version of the signal and an adaptive threshold, typically a running average or rms estimation of the same preprocessed signal, scaled by a gain factor C that provides a sensitivity adjustment.

Since the long term interest of this research is the establishment of a surveillance network against illegal hunting in tropical forest reserves, the analysis of the algorithms is based on a collection of sounds recorded in a dense tropical rain forest, located in Costa Rica's Braulio Carrillo National Park acquired at a 48-kHz sampling rate with 16-bit quantization, on a high-quality digital recorder DVD Fostex PD-6, using a professional high-sensitivity directional Sennheiser MKH416P48V3 microphone [16]. Amplitude is normalized to a maximum pressure of 110 $\mathrm{dB_{SPL}}$. The target samples include five firearms of different calibers, fired at 30, 90, and 250 m from the recording equipment, at angles of 0°, 90°, and 180°. Additional samples for negative validation include a chainsaw recorded at 30 m from the equipment, at the same three angles as the firearms; two planes flying low over the scene; three recordings of various birds singing; two recordings of rain showers; recordings of two different water streams; a recording of wind through the trees surrounding the setting; a Matlab-generated white noise signal with $\sigma^2 = 0.1$; and a male human voice recorded close to the microphone at a normal speech level.

In order to produce an objective selection of the best method for gunshot detection, the selected metric is a receiver operating characteristic (ROC) plot for each preprocessing method, with a final comparison of the best ROCs for each analyzed method. Since the final aim of the project (but not of the work presented in this paper in particular) is to achieve a low-power electronic implementation of the surveillance network, some discussion is added with regard to the hardware complexities of each method, with special emphasis on their power consumption requirements.

Now, according to the signal detection theory [17], the ROC plot is constructed with the ordered pairs (TPR, FPR) of a detection system as a function of a certain detection threshold, where

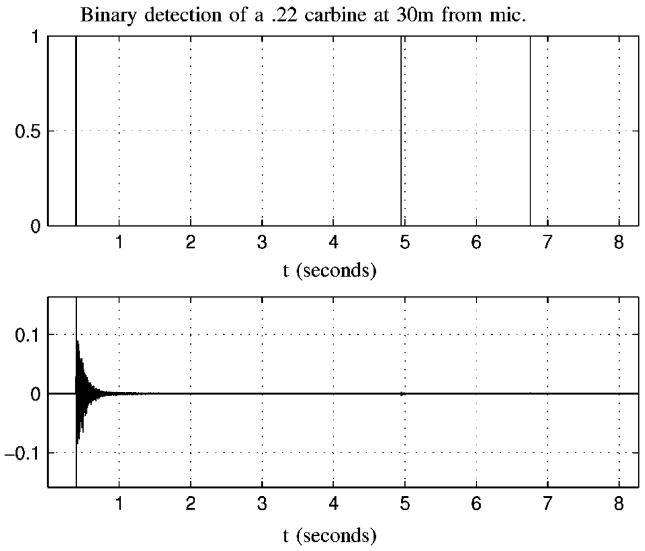

Fig. 4. Positives far away from the real event are considered anomalies that are annotated as the true positive (XTP). In this case, using the TEO as a preprocessing algorithm, for a threshold gain of 40, there are two extra detections showing in the upper image around 4.9 and 6.7 s, which imply that the algorithm is not selective enough.

TPR stands for true positive rate and FPR for false positive rate, and each figure is defined according to

$$TPR = \frac{True\ positives\ detected}{Total\ number\ of\ positives} \tag{1}$$

$$FPR = \frac{False\ positives\ detected}{Total\ number\ of\ negatives}. \tag{2}$$

A true positive is to be considered as such whenever a detection occurs within a few tens of samples of a real gunshot peak impulse. Usually, effective detectors are chosen, allowing for a certain percentage of FPR in order to increase the TPR, since a false positive can always be eliminated later on by the subsequent classification system while a missing true positive is lost forever. This suggests that comparing the algorithms at a fixed FPR may be, statistically speaking, the most efficient way to select the algorithms, using a simple L^1 norm. In our case, nonetheless, a detector with a high FPR would activate additional circuitry, causing extra power consumption. Moreover, it is assumed that the sensor network redundancy can compensate for a certain number of missing true positives. Thus, the evaluation is based on the ordered pair which stands closer (in terms of the Euclidean distance) to a perfect detector with a $(TPR, FPR) = (1, 0)$, where FPR is the x-axis coordinate and TPR is the y-axis coordinate. A discrete ROC with five threshold gain values is calculated for each method, and the best pair is extracted from the plot. In addition, an extra annotation to the true positives, called XTP, is made whenever a positive is generated but not within at least 20 ms from the impulse peak—considering that, in this particular data set, the typical signature's length of a gunshot extended from 60 to 100 ms and the impulsive peak values lay within the first few milliseconds—since this indicates that the algorithm detected something else instead of the searched impulse. An example of a XTP is shown in Fig. 4, while an example of a real positive is shown in Fig. 5.

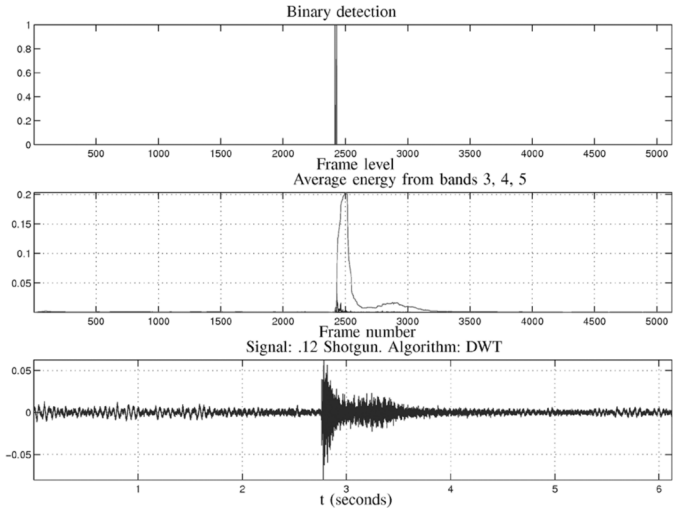

Fig. 5. Example of a correct detection for a .12 shotgun at 250 m from the detector, using the DWT method as the preprocessing algorithm, evaluating the energy in certain frequency bands.

Due to the intended final application of this research, a preliminary hardware implementation is also proposed for the preprocessing methods (except for the adaptive threshold comparison stage, which should be common to all). This provides with another point of comparison between the methods, particularly in regard to their static power dissipation.

III. Description of Preprocessing Algorithms

The following methods are proposed alternatively in [5], [11], and [15]. Applying the signal directly to the threshold detector, with no signal preprocessing at all, is taken as an evaluation reference (i.e., as the metric's lower bound: the rest of the methods should give results above it). Signals are prefiltered using an IIR fourth-order Butterworth low-pass filter with a cutoff frequency of 3 kHz (determined from the observation of the gunshots' power spectra), except those to be processed using wavelets, where the filtering is done by the processing itself. In the case of the negative samples, signals are taken to amplitude levels equivalent to sound pressures ranging between 90 $\mathrm{dB_{SPL}}$ and 98 $\mathrm{dB_{SPL}}$ (the typical pressure levels of gunshots at distances greater than 90 m from the gun barrel, on an obstacle-free propagation environment).

Now, since the signals are of a particularly high intensity with regard to other sounds in the surroundings, the possible influence of electronic noise in the intended hardware implementations is deemed as insignificant. Moreover, distortion is not considered a factor, since signals arrive already distorted to the sensors due to inevitable multipath interference and the signal's high intensity that, in some cases, even saturates the receiving microphone.

A. Absolute Value

The absolute value of the input signal is taken before being introduced into the detection scheme in Fig. 3. Since $abs[x(t)]$ is a one-to-one mapping of the energy estimation of the signal $(x^2(t))$, their respective performances are considered to be equivalent (as Obeid and Wolf argue in [15]), but with a lower implementation complexity than that of a squarer/multiplier.

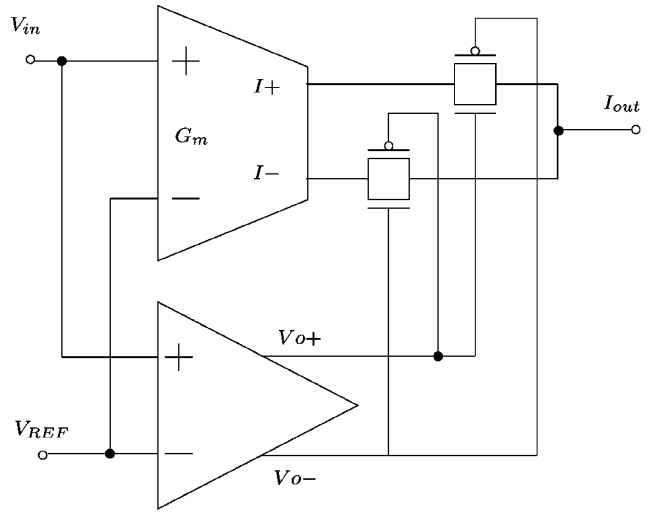

Fig. 6. Simple low-power CMOS rectifier. The $I_{\rm bias}$ for this circuit is on the order of 405 nA, with a 1-V linear range (see [23] and [24]). An extra single-ended OTA is used as a current–voltage converter.

TABLE I
BIAS CURRENT CONSUMPTION FOR THE PROPOSED ABSOLUTE-VALUE CIRCUIT, USING THE RECTIFIER PROPOSED IN [23] AND IMPLEMENTED IN [24] ON A 0.5-μm STANDARD CMOS TECHNOLOGY. RESULTS ARE BASED ON SPICE SIMULATIONS

SubCircuit	Qty	Bias Current
Dual OTA	1	270nA
Comparator	1	45nA
Single-ended OTA	1	90nA
	Total I_{BIAS}	405nA

There are plenty of analog multiplier structures in the literature [18]–[21], but as Han and Sánchez-Sinencio discuss in [22], most of them can be grouped on a few categories; as they show, effective multipliers with low distortion and a good linear range always require extra circuitry to provide for common mode shifting. On the other hand, the absolute value of a signal can be performed by a simple analog rectifier. An example of such circuit is shown in Fig. 6, as proposed in [23]. This rectifier only needs a dual operational transconductance amplifier (OTA) and a comparator, plus another OTA for current–voltage conversion (not shown). From simulations, the circuit is found to have a linear range over 1 V and requires only 405 nA (see Table I), implemented on a 0.5-μm standard CMOS technology (see [24]). An alternative is to use four quadrant multipliers with floating-gate MOS transistors that use low-voltage supplies and have an extended linear range (see [25]–[28] for a few examples); this alternative might be considered in the future.

B. Median Filter

The input signal is fed into a delay chain with six taps, where each tap inserts a 1-ms delay to the signal. The input signal and the six outputs of each delay tap form a searching window of size seven, which is fed to a median filter whose output is subtracted from the signal after the third delay tap (i.e., the middle of the window); this is considered as the normalized energy that enters into the threshold unit (Fig. 7). The implemented median filter is of the form

$$y(n) = \underset{i=0,\ldots,6}{\text{median}}\{x(n - i\Delta_n)\} \tag{3}$$

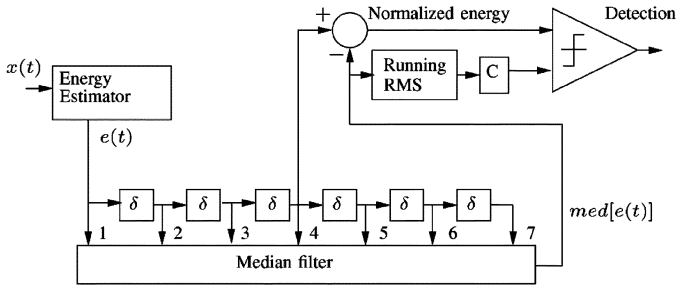

Fig. 7. Median filter structure. The time delay taps (δ) implement the window for the filter. Since there is a one-to-one relation between $x^2(t)$ and $abs[x(t)]$, the second method is used because it is easier to implement in analog or sampled-time approaches.

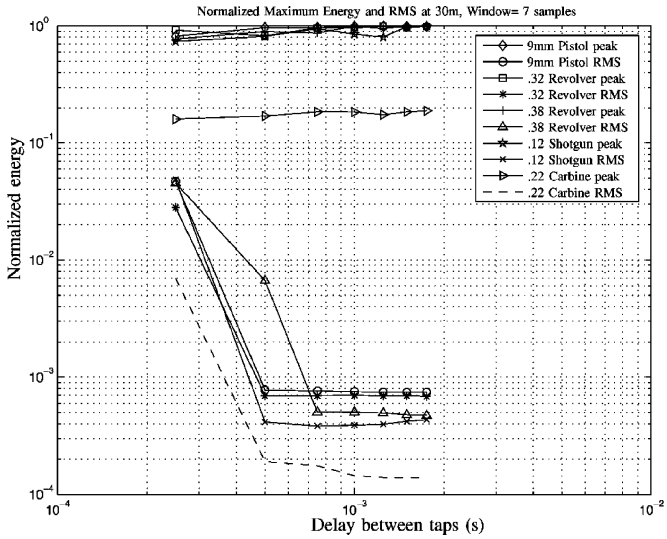

Fig. 8. For a median filter with a window of size seven, the peak values of energy of each signal after the filtering are plotted together with their respective energy's rms running average as a function of the delay between taps. It is clear that, beyond a 1-ms delay, the improvement in the differences of energy is not significant.

where $\Delta_n = F_s \cdot 1\,\text{ms}$ and $F_s = 48\,\text{kHz}$. In general, the behavior of the median filter is similar to that of a low-pass filter, as it smooths the signal but preserves abrupt changes (and therefore, it passes some high frequencies too).

Dufaux *et al.* [5] proposed this structure using a median filter with a window size of 20, using a 44.1-kHz sampling rate with 24-bit data resolution. This means a 20-tap delay chain with a 22-μs delay time.

In this case, in order to choose the length for the window and the delay separation between each tap, some simulations were performed with the available gunshot signals. The idea was to find a maximum difference between the energy peak of each signal and its normalized energy's running rms average as a function of the window's length and the delay between taps. From the plot of the results, it was possible to determine the chosen window size of seven with the used delay of 1 ms for each tap (Fig. 8 shows one of the plots used for the determination of these parameters: It is clear that beyond 1 ms, the improvement in the differences of energy is not significant).

For our purposes, a digital implementation is not possible due to its high area and power requirements, particularly regarding the needed sorting algorithm for the median calculation. A completely analog implementation as in [29] and [30] is constrained

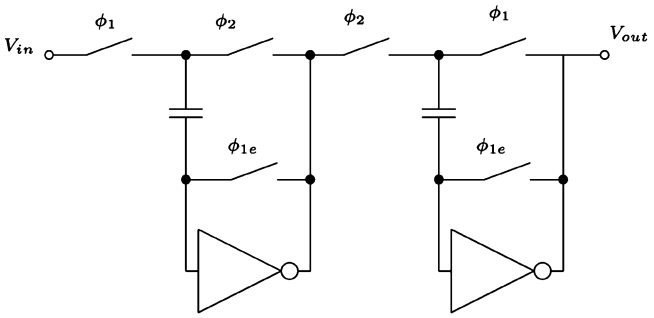

Fig. 9. Basic delay unit. Signal is sampled and held using two nonoverlapped clocks [32]. An analog chain register may be built using this structure.

TABLE II
BIAS CURRENT CONSUMPTION FOR THE POSSIBLE IMPLEMENTATION OF A MIXED-SIGNAL MEDIAN FILTER, WITH A CHAIN OF TIME DELAYS AS PROPOSED IN [32], PORTED TO A 0.5-μm STANDARD CMOS TECHNOLOGY. BIAS RESULTS BASED ON THE DATA FROM THE SUBCIRCUITS PROPOSED IN [24] BUT USING THE TOPOLOGY PROPOSED IN [29]

Sub-circuit	Qty	Bias Current
Single-ended OpAmps	14	2.8μA
Diff. OpAmps	7	315nA
Rectifier (as defined in Table I)	1	405nA
	Total I_{BIAS}	3.52μA

by the delay of the taps in the chain, which is on the order of 1 ms. Typical analog versions of delay chains are based on all-pass filters, which at best provide delays equivalent to a phase shift of up to π radians of the input signal. Moreover, delay constants on the order of hundreds of microseconds require RC relations that are hard to achieve on standard CMOS processes. A sampled-time approach is therefore a reasonable alternative. A bucket-brigade device (BBD) may serve as the delay chain. The search window, nonetheless, must be limited in length, as this structure quickly degrades the signal [31]. A better option in terms of signal conservation is the use of a delay chain, as proposed in [32] and shown in Fig. 9. A bigger area and, therefore, a higher power dissipation are the price to pay: Two operational amplifiers are needed per stage [the use of single-ended cascode telescopic Operational Amplifiers (OpAmps), as proposed in [33], substantially cuts power and area requirements]. This means 14 single-ended OpAmps just for the delay stage (with a 200-nA bias current for each OpAmp on a 0.5-μm CMOS process [32], [33]) and seven differential OpAmps for the analog median filter operation using the topology in [29], with a 45-nA bias current for each, if the OpAmps proposed in [24] are used on the same technology. Table II gives the details. This of course disregards the discretization of the input signal by the delay chain, which implies verification if the use of a continuous median filter for the sorting is still valid.

C. TEO

The Teager energy operator (TEO), as defined in [34], is applied to the signal before feeding it to the threshold unit. This operator has the following discrete form:

$$y(n) = x(n)^2 - (x(n-1)x(n+1)) \tag{4}$$

which, as reported by [34], enhances the high-frequency components of the input signal $x(n)$ and is thus recommended for the detection of impulsive signals. Its discrete time implementation is shown in Fig. 10.

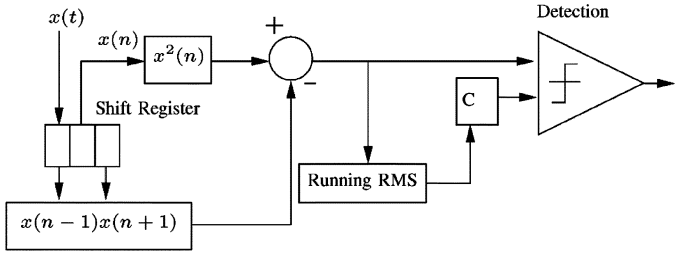

Fig. 10. TEO basic structure.

TABLE III
BIAS CURRENT CONSUMPTION FOR THE POSSIBLE IMPLEMENTATION OF AN ANALOG TEO ALGORITHM, AS PROPOSED IN [35], PORTED TO A 0.5-μm STANDARD CMOS TECHNOLOGY. BIAS RESULTS BASED ON THE DATA FROM THE SUBCIRCUITS PROPOSED IN [24]

Sub-circuit	Qty	Bias Current
Single-ended OTA	11	990nA
Multipliers	2	180nA
	Total I_{BIAS}	1.170μA

One advantage of this method is that it can be approximated by an analog circuit, following the continuous equation also given in [34]

$$y(t) = \left(\frac{dx(t)}{dt}\right)^2 - x(t)\frac{d^2x(t)}{dt^2}. \tag{5}$$

A particular proposal for action potential detection is offered in [35]. Two bulk-driven multipliers are used, plus two $Gm{-}C$-based differentiators. Table III shows an approximation in terms of the number of needed subcircuits and the required bias, considering a 0.5-μm implementation of the circuit given in [35], with the subcircuits' bias requirements given in [24]. The small linear range of the multipliers (200 mV, as reported in [35]) is a problem to be dealt with if this topology is chosen.

D. Correlation Against a Template

Detection and classification methods based on correlation matching are common in plenty of fields, from brain machine interfaces [15] to ultrawideband receivers [36]. Digital simplified detectors based on correlation with very low power dissipation have been successfully built for particular applications [37], and mixed-signal general classifiers have also been proposed [31]. Here, a full-scale method is initially proposed (16-bit resolution and 48-kHz sampling rate) as a top metric for the evaluation of the method's efficiency. On a later stage, simplifications such as the use of integer arithmetic with lower resolution or a lower sampling may be introduced in order to gauge the tradeoffs between the degrading efficiency of the method and its hardware feasibility.

The detection structure is shown in Fig. 11. First, two signal templates are obtained by the averaging of gunshot signals at 30 and 90 m, as Obeid and Wolf propose [15]. The templates are stored in two 1000-sample long vectors. Signal is fed through a window with the same size of the template vectors, at a rate of 39 samples per iteration. At each iteration, correlation with each vector is computed and stored in another pair of vectors. These

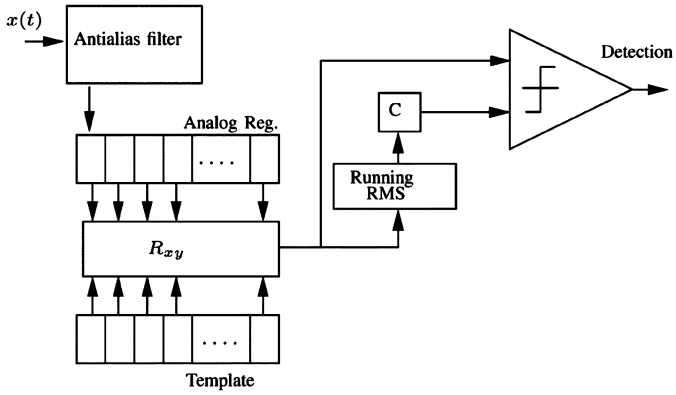

Fig. 11. Basic scheme for a discrete correlation-based detection algorithm.

are the outputs of the system, which go to a threshold detector. Since the correlation is a signed operation, the averaging is done using a running rms scheme.

Since the gunshot response is highly dependent on the environment, it is clear that the correlation might be affected by such environmental effects. Nonetheless, as the wilderness region where the signals were gathered is homogenous enough and highly representative of the areas where the results of this research are to be applied, no data were gathered from other places. However, provisions were taken to acquire the signals at different distances and angles of incidence with respect to the microphone. It is also clear that, at least regarding the correlation algorithm, different data would be necessary if the intended system were to be used in locations with different environmental conditions as the ones here indicated.

In terms of a possible hardware implementation, going strictly digital is prohibitive because of the expensive digital multiplication structures and the temporal storing needed. Subquantization was applied in order to search for simpler digital implementations but just going from 16- to 8-bit degraded performance, with the FPR increasing to almost 0.3 to 0.4 in most cases. A plausible alternative is Edwards and Cauwenberghs' proposal of a mixed-mode implementation of this algorithm [31], with a reported consumption of 50 to 30 μW. Here, the computation is not done directly on the signal itself but on the features provided by a wavelet, cochlear or any other kind of preprocessing algorithm. The sampling vector used is a BBD structure of 64 taps, and the correlation is done by an analog current multiplication of the input with a binary pattern. Just as in the median filter case, the main limitation arises from the fact that the BBD cannot be very long. This entails shortening of the template as well (from 1000 to 64 taps in our case) and a cut on the sampling frequency. On the other hand, a delay chain, as proposed in [32], may be used, i.e., 128 single-ended single-stage OpAmps just in the delay chain, with the corresponding power consumption increase. Table IV shows the static power requirements of a possible implementation, ported to a 0.5-μm technology and with the changes indicated before, using data from the subcircuits proposed in [24] and [32].

E. DWT

Istrate *et al.* propose in [11] the use of discrete analysis with a Daubechies wavelet of six vanishing moments for the detection

TABLE IV
BIAS CURRENT CONSUMPTION FOR A POSSIBLE IMPLEMENTATION OF THE MIXED-SIGNAL CORRELATION, AS PROPOSED IN [31], BUT WITH THE SUBSTITUTION OF THE BBD CHAIN FOR A CHAIN OF SAMPLERS, AS PROPOSED IN [32], PORTED TO A 0.5-μm STANDARD CMOS TECHNOLOGY. BIAS RESULTS BASED ON THE DATA FROM THE SUBCIRCUITS PROPOSED IN [24] AND [32]

Sub-circuit	Qty	Bias Current
Single-ended OpAmps	128	25.6μA
Diff. OpAmps	3	135nA
64-bit SRAM	1	≈ 0
	Total I_{BIAS}	25.74μA

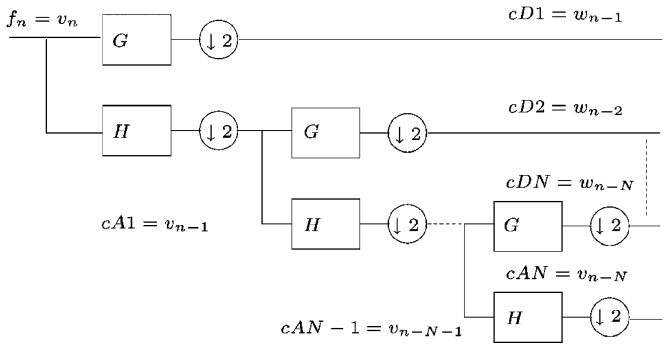

Fig. 12. General structure of a wavelet decomposition bank filter. Signal details are given by the w_n coefficients. Signal is approximated by the v_n coefficients.

of impulsive signals. According to [38] and [39], a real conjugate mirror filter h such that $H(\omega)$ (the Fourier transform of h) has p zeros at $\omega = \pi$ and has at least $2p$ nonzero coefficients. Furthermore, to ensure that a wavelet has p vanishing moments, $H(\omega)$ must have a zero of order p at $\omega = \pi$. A Haar wavelet has one vanishing moment and, therefore, its support is two, while a Daubechies wavelet of six vanishing moments has a support of 12 nonzero coefficients. Hence, the computational complexity of computing the output with FIR filters is six times higher under the assumption that all multipliers have the same cost. Haar computation can be further improved, as the coefficients are equal in magnitude, which reduces the number of products by 1/2. Thus, in this case, an eight-level Haar wavelet bank filter is used on a 7-kHz subsampled signal. Fig. 12 shows the filter bank recursive structure, following Mallat's notation [38].

The filter bank is structured following a dyadic scale using 3500 Hz as the Nyquist frequency, and the inputs to this filter are 2048 length sequences. The number of levels to be used in the decomposition and the choice of the coefficients of interest are the result of preliminary analysis with the wavelet interactive Matlab toolbox. The energy of the chosen coefficients is calculated using two alternative methods: squaring the signal or obtaining its absolute value. After evaluating different cases, it was concluded that the best results are obtained considering levels 3, 4, and 5 and levels 4, 5 and 6. The output is then used as input to the threshold detector, as shown in Fig. 13. The choice of Haar functions is based on their simple form, which allows mixed-mode hardware implementation using switched capacitors, for instance. A Haar scale function is related to a moving average operator with a transfer function $H(z) = (1 + z^{-1})/\sqrt{2}$, while its wavelet function gives rise to a moving difference operator with a transfer function $G(z) = (1-z^{-1})/\sqrt{2}$.

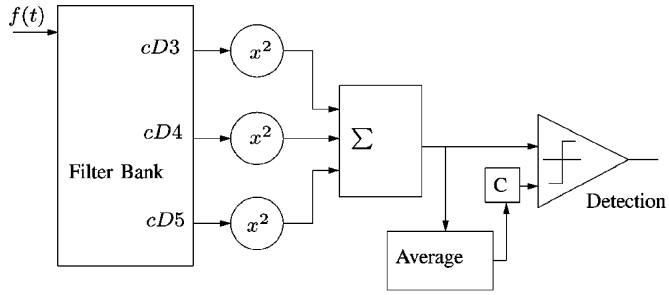

Fig. 13. Wavelet filter bank structure. The energy of each detail coefficient is calculated before feeding it to the energy adder. Energy may be estimated by a squaring or absolute-value estimator.

TABLE V
BIAS CURRENT CONSUMPTION FOR THE IMPLEMENTATION OF A HAAR WAVELET BANK FILTER ON A 0.5-μm STANDARD CMOS PROCESS, USING PRELIMINARY RESULTS FROM [24]

Sub-circuit	Qty	Bias Current
Single-ended OpAmps	16	3.2μA
Energy calculation unit (estimated)	1	1.5μA
	Total I_{BIAS}	4.7μA

The $\sqrt{2}$ factor ensures the orthonormality of the wavelet transformation and may be replaced by another factor, considering that only the analysis of the signals is required, not their reconstruction.

A possible hardware implementation on a 0.5-μm standard CMOS process for the wavelet bank filter is given in [24], where the recursive filter is replaced with an equivalent parallel implementation. Preliminary data power, based on some tests and simulations, is given in Table V.

F. CWT

A discrete wavelet analysis is generally done using a recursive filter bank. However, a completely digital implementation of such a filter may be expensive in terms of area and power dissipation. An alternative mixed-signal solution using Haar filters and a parallel topology instead of a recursive one may result in a more efficient architecture. Another option is the use of a continuous wavelet transform (CWT), using functions such as Morlet or Gauss wavelets, as proposed in [29] and [40]–[44]. However, as shown in the literature, the electronic implementation of these wavelets is complex and not straightforward. A simpler approach is to reduce the transfer functions of each filter to a passband expression in a similar way to cochlear filter banks but using a parallel structure instead of a recursive one. As it has been shown, a cochlear filter bank provides a time–frequency decomposition equivalent to that of a wavelet analysis [45]–[48]. Thus, a continuous filter version of the wavelet analysis is proposed, with third- or fourth-order passband filters, following the same topology shown in Fig. 13. The frequency tiling is obtained by scaling the cutoff frequencies just like in the discrete case. Thus, a parallel filter bank with three different passband frequencies is defined, as shown in Fig. 14. The chosen frequency ranges are determined by the previous discrete wavelet transform (DWT) analysis, which determined that coefficients 3, 4, 5 and 4, 5, 6 of an eight-level wavelet decomposition are enough for the intended purposes of detection.

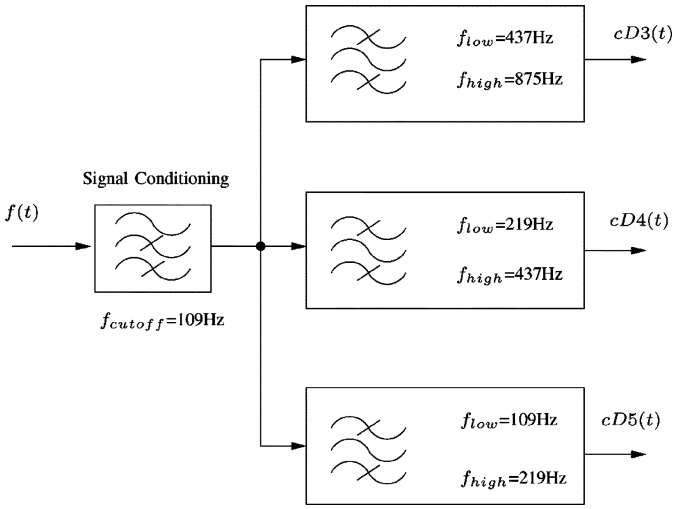

Fig. 14. Analog parallel bank filter, equivalent to a CWT analysis. Cutoff frequencies are based on the dyadic division obtained by the DWT analysis. All passband filters are of third order, with a first-order high-pass input filter for signal conditioning.

Thus, the resulting transfer function for each passband filter is given by

$$CD(s)_n = \frac{\frac{2^n s}{\omega_1}}{\left(1+\frac{2^{n-1}s}{\omega_1}\right)^2\left(1+\frac{2^n s}{\omega_1}\right)} \tag{6}$$

where n determines the corresponding coefficient. In order to get rid of any offset and $1/f$ noise, an extra first-order high-pass filter is placed at the system's input. Simulations are performed using Matlab's LTI toolbox (Fig. 15).

An extra consideration was taken into account regarding energy estimation in the wavelet algorithms: The first analysis was done using a squaring estimator. Then, another analysis was performed using an absolute-value estimator. Results showed that the absolute-value estimator did not degrade noticeably the effectiveness of the methods, even considering the loss of the impulsive strengthening that a square estimator should produce. This result implies a significant hardware simplification (considering the complexities of analog and discrete multipliers already discussed in Section III-A). Moreover, a secondary benefit was the need for lower gains in the adaptive threshold unit, of at least one order of magnitude. Although counterintuitive at the first glance, this lower gain is due to the normalized input signals, which entailed a compressive effect instead of an expanding one for the squaring unit, something that would still apply for its intended hardware implementation, considering the use of voltages on the order of hundreds of millivolts.

A $Gm{-}C$ hardware implementation of this circuit is given in [24], ported to a 0.5-μm standard CMOS process. Currently, this implementation is under testing with the same data set used for the evaluation of the algorithms. Results will be offered in another publication. Preliminary power data are summarized in Table VI (based on measurements).

IV. EVALUATION RESULTS AND ALGORITHM RANKING

Detection was evaluated for different gains. An example of such evaluation is shown in Fig. 5 for the discrete Haar wavelet

TABLE VI
BIAS CURRENT CONSUMPTION FOR THE IMPLEMENTATION OF A CWT BANK FILTER ON A 0.5-μm STANDARD CMOS PROCESS. BIAS RESULTS BASED ON REAL MEASUREMENTS [24]

Sub-circuit	Qty	Bias Current
Single-ended OTA	14	2.160μA
Rectifier (as defined in Table I)	3	1.215μA
	Total I_{BIAS}	3.375μA

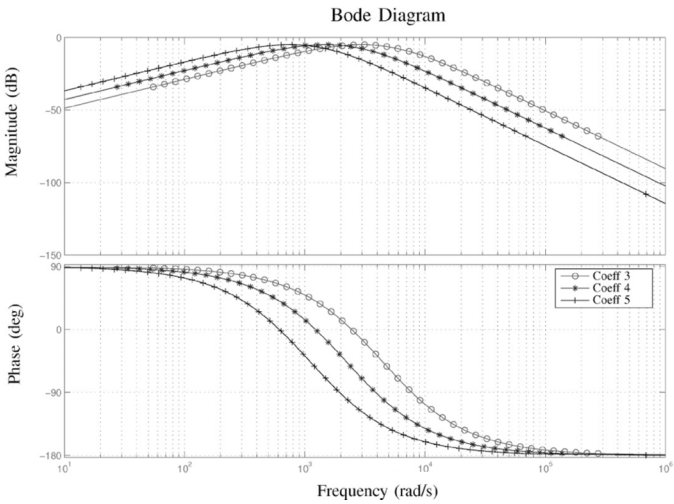

Fig. 15. Theoretical frequency responses for the filters shown in Fig. 14, using Matlab's LTI toolbox.

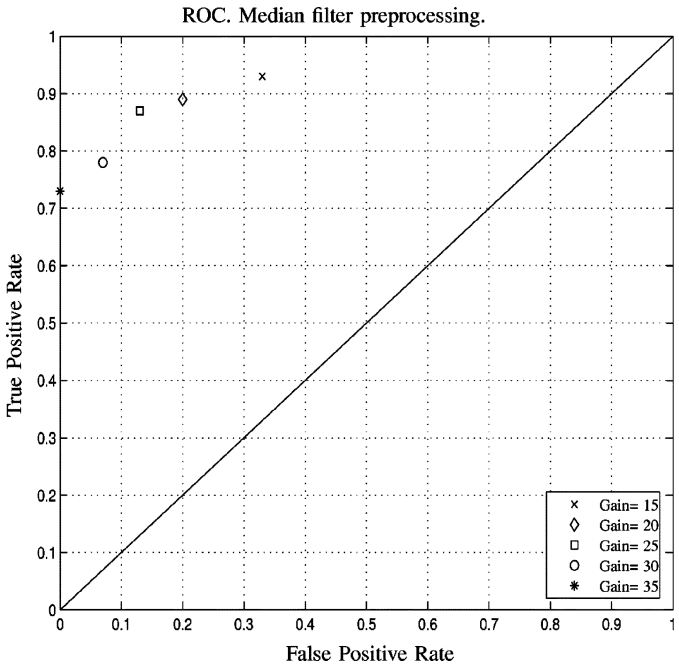

Fig. 16. Sample of the ROC for an adaptive threshold detector with median filter preprocessing.

algorithm. With the results from the evaluation of the 45 positive samples, plus the 15 negative samples, ROCs were plotted for each method. An example of such plots is shown in Fig. 16. Table VII shows the ranking of the best pairs for each tested method, with the corresponding gain C for the threshold unit.

For each algorithm, the best (TPR, FPR) was chosen (with its associated gain) in terms of the Euclidean distance between each (TPR, FPR) pair and the ordered pair that represents a perfect detector $(TPR, FPR) = (1, 0)$: the smaller the distance, the better the algorithm. Table VII lists the best algorithms in descending order of its effectiveness (i.e., in descending order of the Euclidean distance from a perfect detector). Next to each algorithm, XTPs are also indicated, since they also qualify each method, i.e., serve as an extra indicator to eliminate ties in the rating. Ideally, no XTPs should exist.

TABLE VII
BEST ROC (TPR, FPR) PAIRS PER ALGORITHM IN TERMS OF THEIR EUCLIDEAN DISTANCE FROM A PERFECT DETECTOR $(TPR, FPR) = (1, 0)$). NEXT TO EACH ALGORITHM, THE REQUIRED GAIN FOR THE ADAPTIVE THRESHOLD DETECTOR IS ALSO GIVEN

Method	TPR	FPR	Distance	XTP	Gain
Correlation 30m template	41/45	0/15	0.088	1	25
Correlation 90m template	41/45	0/15	0.088	1	25
Discrete Wavelet Transform Bands 3, 4, 5 with absolute value as energy estimator	40/45	0/15	0.111	0	15
Continuous Wavelet Transform Bands 3, 4, 5 with absolute value as energy estimator	40/45	1/15	0.129	0	30
Continuous Wavelet Transform Bands 3, 4 with absolute value as energy estimator	40/45	1/15	0.129	3	30
Median Filter	39/45	2/15	0.189	0	25
Discrete Wavelet Transform Bands 4, 5, 6 with absolute value as energy estimator	37/45	1/15	0.190	0	10
Absolute Value Estimator	38/45	2/15	0.205	0	15
No Pre-processing	35/45	2/15	0.259	0	15
TEO	36/45	3/15	0.283	2	45

According to the ROC ranking, correlations against templates at 30 or 90 m were the two best preprocessing methods, yielding no false positives but with two XTPs. The third method was the DWT with an absolute-value estimator, using detail coefficients 3, 4, and 5, with no false positives and no XTPs. In the fourth place was the CWT for coefficients 3, 4, and 5, with an FPR of only 1/15 (a false positive due to the rain sample number two and no XTPs). In the fifth place was also the CWT, but only considering bands 3 and 4, with three XTPs (which seems to indicate that the fifth coefficient may be left unconsidered if one is to optimize hardware area at the cost of higher FPR). The sixth algorithm in terms of effectiveness was the median filter. In the seventh place was the DWT for bands 4, 5, and 6, with an absolute-value estimator. In the eighth place was the absolute-value estimator. At the end of the table is the TEO, which did not even surpass the metric's lower bound of no preprocessing method at all.

The posterior analysis of the negative samples that produced some of these false positives showed strong "pops" in the recording (see, for instance, Fig. 17), which were probably caused by water drops hitting the microphone and generating an impulsive sound. An acoustic protection on the microphone could thus increase the TPR while decreasing the FPR. Anyway, it is remarkable that the correlation and the wavelet algorithms are not fooled by these pops. Taking the absolute value of the signal outperformed the TEO operator not only in its TPR but also in its FPR, which coincides with the Obeid and Wolf observations that included even more refined versions of the latter method [15]. As in the median filter case, the pops' effect in the negative samples is present in both methods, which

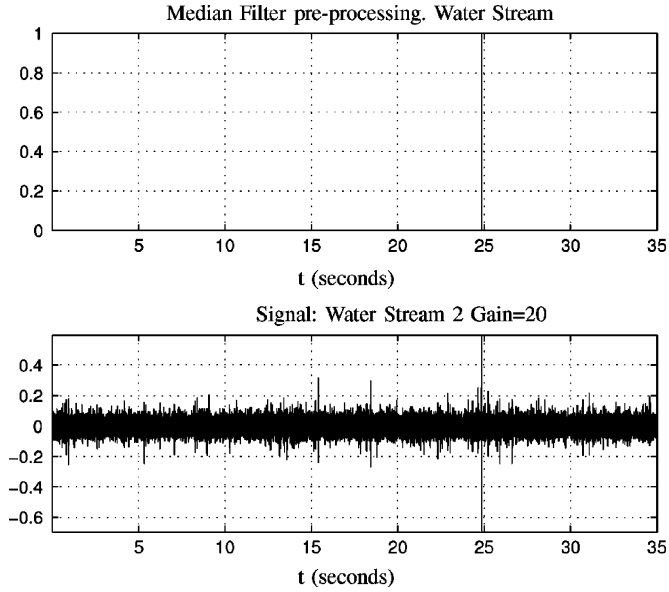

Fig. 17. False positive using the median filter on a water stream recording. Notice the pop in the sample that fools the algorithm. A higher gain in the threshold detector circumvents the false positive, at the expense of losing some true positives. An acoustic protection on the microphone may be a simple solution for this false positive without sacrificing the TPR.

TABLE VIII
RANKING OF THE METHODS AS A FUNCTION OF THEIR REQUIRED BIAS. DYNAMIC POWER CONSUMPTION IS NOT CONSIDERED

Method	Total Bias Current
Absolute Value	405nA
Teager Energy Operator	1.170μA
Continuous Wavelet	3.375μA
Median Filter	3.52μA
Haar Discrete Wavelet	4.7μA
Mixed signal correlator	25.74μA

means that a similar protection of the microphone may increase their performance. Not considering, for instance, the negative sample of the water stream brings the FPR down to 1/15 in the absolute-value preprocessing, the same as in the second case of the wavelet method.

Table VIII tabulates some of the annotations given regarding the approximate static power requirements of the possible implementation of each method. Considering this, it is clear that both the TEO and absolute-value algorithms may compensate their low detection performance in terms of their lower power needs against the higher power requirements of the other methods. However, if one is to prefer a more detection-effective method, then it seems better to opt for the more power-demanding algorithms.

A compromise solution in terms of power efficiency thus may be offered by a discrete implementation of the DWT, using a switched capacitor approach, for instance, or the implementation of the CWT method using a $Gm{-}C$ or equivalent approach.

At the time of submission of this paper, the continuous wavelet IC implementation was being tested on laboratory. The second version, which is a partial implementation of the discrete wavelet approach, has just returned from the foundry. The results of these two circuits' testing will be the object of a subsequent publication that will complement the results presented in this paper.

V. CONCLUSION

Detection of impulsive signals can be implemented with a variety of effective algorithms. An ROC statistical metric has been proposed in order to sort them in terms of detection efficiency, and some annotations have been given about their VLSI low-power feasibility. Clearly, correlation and wavelet-based detection algorithms give higher performances at a higher hardware cost, at least in terms of static power consumption. There exist good mixed-signal and analog approaches to the VLSI implementation of wavelet-based methods that would suggest this as the best compromise solution. A median filter approach may be not as hardware costly as the preceding methods, with detection results still acceptable. For that matter, just considering the absolute value of the signal, with a protected microphone, can offer a similar performance at a much lower hardware cost.

REFERENCES

[1] R. Maher, "Modeling and signal processing of acoustic gunshot recordings," in *Proc. 2nd Signal Process. Educ. Workshop, 4th Digital Signal Process. Workshop*, 2006, pp. 257–261.
[2] R. Maher, "Acoustical characterization of gunshots," in *Proc. IEEE Workshop Signal Process. Appl. Public Security Forensics, SAFE*, 2007, pp. 1–5.
[3] P. Weissler and M. T. Kobal, "Noise of police firearms," *J. Acoust. Soc. Amer.*, vol. 56, no. 5, pp. 1515–1522, Nov. 1974.
[4] R. Stoughton, "Measurements of small-caliber ballistic shock waves in air," *J. Acoust. Soc. Amer.*, vol. 102, no. 2, pp. 781–787, Aug. 1997.
[5] A. Dufaux, L. Besacier, M. Ansorge, and F. Pellandini, "Automatic sound detection and recognitions for noisy environment," in *Proc. X EUSIPCO*, 1997, p. 1889.
[6] K. Molnar, A. Lédeczi, L. Sujbert, and G. Peceli, "Muzzle blast detection via short time Fourier transform," in *Proc. 12th PhD Mini-Symp.*, 2005, pp. 16–17.
[7] B. Sadler, L. Sadler, and T. Pham, "Optimal and robust shockwave detection and estimation," in *Proc. IEEE ICASSP*, 1997, vol. 3, pp. 1889–1892.
[8] B. Ferguson, L. Criswick, and K. Lo, "Locating far-field impulsive sound sources in air by triangulation," *J. Acoust. Soc. Amer.*, vol. 111, no. 1, pt. 1, pp. 104–116, Jan. 2002.
[9] G. Duckworth, J. Barger, S. Carlson, D. Gilbert, M. Knack, J. Korn, and R. Mullen, "Fixed and wearable acoustic counter-sniper systems for law enforcement," in *Proc. SPIE Int. Symp. Enabling Technologies for Law Enforcement and Security Sensors, C3I, Information, and Training Technologies for Law Enforcement*, 1998, pp. 3575–3577.
[10] A. Lédeczi, P. Volgyesi, M. Maroti, G. Simon, G. Balogh, A. Nodas, B. Kusy, S. Dora, and G. Pap, "Multiple simultaneous acoustic source localization in urban terrain," in *Proc. 4th Int. Symp. Inf. Process. Sensor Netw.*, Los Angeles, CA, 2005, p. 69.
[11] D. Istrate, E. Castelli, M. Vacher, L. Besacier, and J. F. Serignat, "Information extraction from sound for medical telemonitoring," *IEEE Trans. Inf. Technol. Biomed.*, vol. 10, no. 2, pp. 264–274, Apr. 2006.
[12] M. Zu, P. Su, R. Shi, W. Wang, and J. Yu, Intelligent tracer of hunting activities Lily Studio, Univ. Nanjing. Nanjing, China, Jun. 2006.
[13] A. I. T. Fernández, "Propagación del sonido en bosques. Análisis comparativo de las medidas in situ, en laboratorio y de los valores predichos por un modelo," Ph.D. dissertation, Universidad de Valladolid, Valladolid, España, 2002.
[14] A. Chacon-Rodriguez and P. Julian, "Evaluation of gunshot detection algorithms," in *Proc. Argentine School Micro-Nanoelectron., Technol. Appl., EAMTA*, 2008, pp. 49–54.
[15] I. Obeid and P. Wolf, "Evaluation of spike-detection algorithms fora brain–machine interface application," *IEEE Trans. Biomed. Eng.*, vol. 51, no. 6, pp. 905–911, Jun. 2004.
[16] *"Sennheiser MKH416P48U3 Datasheet"* Sennheiser, Old Lyme, CT, 2005 [Online]. Available: http://www.bfm.ee/web/data/www_files/facilities/manuals/SENNHEISER-MKH416-Boom-Microphone-SPECIFICATIONS.pdf

[17] D. Heeger, Signal detection theory Stanford Univ., Stanford, CA, 1997.
[18] A. Demosthenous and M. Panovic, "Low-voltage MOS linear transconductor/squarer and four-quadrant multiplier for analog VLSI," *IEEE Trans. Circuits Syst. I, Reg. Papers*, vol. 52, no. 9, pp. 1721–1731, Sep. 2005.
[19] H. Song and C. Kim, "A MOS four-quadrant analog multiplier using simple two-input squaring circuits with source followers," *IEEE J. Solid-State Circuits*, vol. 25, no. 3, pp. 841–848, Jun. 1990.
[20] M. Craven, B. Hayes-Gill, and K. Curtis, "Two quadrant analogue squarer circuit based on MOS square-law characteristic," *Electron. Lett.*, vol. 27, no. 25, pp. 2307–2308, Dec. 1991.
[21] I. Filanovsky and H. Baltes, "CMOS two-quadrant multiplier using transistor triode regime," *IEEE J. Solid-State Circuits*, vol. 27, no. 5, pp. 831–833, May 1992.
[22] G. Han and E. Sanchez-Sinencio, "CMOS transconductance multipliers: A tutorial," *IEEE Trans. Circuits Syst. II, Analog Digit. Signal Process.*, vol. 45, no. 12, pp. 1550–1563, Dec. 1998.
[23] A. Arnaud, "Very large time constant $Gm-C$ filters," Ph.D. dissertation, Universidad de la República, Uruguay, Montevideo, Uruguay, 2002.
[24] A. Chacón-Rodríguez, "Circuitos integrados de bajo consumo para detección y localización de disparos de armas de fuego," Ph.D. dissertation, Universidad Nacional de Mar del Plata, Mar del Plata, Argentina, 2009.
[25] S. Vlassis and S. Siskos, "Analogue squarer and multiplier based on floating-gate MOS transistors," *Electron. Lett.*, vol. 34, no. 9, pp. 825–826, Apr. 1998.
[26] J. Ramirez-Angulo, S. Choi, and J. Zrilic, "Compact modular expandable analog defuzzifiers using multiple input floating gate transistor transconductance multipliers," in *Proc. IEEE ISCAS*, Geneva, Switzerland, 2000, vol. 5, pp. 381–384.
[27] S. Garimella, J. Ramirez-Angulo, A. Lopez-Martin, and R. Carvajal, "Design of highly linear multipliers using floating gate transistors and/or source degeneration resistor," in *Proc. IEEE ISCAS*, May 18–21, 2008, pp. 1492–1495.
[28] S. Keles and H. Kuntman, "Four quadrant FGMOS multiplier," in *Proc. Int. Conf. ELECO*, Nov. 5–8, 2009, pp. II-45–II-48.
[29] C. Sanchez-Lopez, A. Diaz-Sanchez, and E. Tlelo-Cuautle, "Analog implementation of MOS-translinear Morlet wavelets," in *Proc. ISCAS*, 2003, vol. 1, pp. I-393–I-396.
[30] I. Opris and G. Kovacs, "A high-speed median circuit," *IEEE J. Solid-State Circuits*, vol. 32, no. 6, pp. 905–908, Jun. 1997.
[31] R. Edwards and G. Cauwenberghs, "Mixed-mode correlator for micropower acoustic transient classification," *IEEE J. Solid-State Circuits*, vol. 34, no. 10, pp. 1367–1372, Oct. 1999.
[32] M. Stanacevic and G. Cauwenberghs, "Charge-based CMOS FIR adaptive filter," in *Proc. 43rd IEEE Midwest Symp. Circuits Syst.*, 2000, vol. 3, pp. 1410–1413.
[33] M. Stanacevic, K. Murari, A. Rege, G. Cauwenberghs, and N. Thakor, "VLSI potentiostat array with oversampling gain modulation for wide-range neurotransmitter sensing," *IEEE Trans. Biomed. Circuits Syst.*, vol. 1, no. 1, pp. 63–72, Mar. 2007.
[34] J. Kaiser, "Some useful properties of Teager's energy operators," in *Proc. IEEE ICASSP*, 1993, vol. 3, pp. 149–152.
[35] B. Gosselin and M. Sawan, "An ultra low-power CMOS action potential detector," in *Proc. IEEE ISCAS*, 2008, pp. 2733–2736.
[36] T. Kaiser, "Spatial aspects of UWB," in *UWB Communication Systems*. New York: Hindawi, 2006, pp. 253–410.
[37] D. H. Goldberg, A. G. Andreou, P. Julián, P. Pouliquen, L. Riddle, and R. Rosasco, "VLSI implementation of an energy-aware wake-up detector for an acoustic surveillance sensor network," *ACM Trans. Sens. Netw.*, vol. 2, no. 4, pp. 594–611, Nov. 2006.
[38] S. G. Mallat and S. Mallat, *A Wavelet Tour of Signal Processing*. New York: Academic, 1998.
[39] A. Bultheel, Wavelets With Applications in Signal and Image Processing 2008.
[40] S. Haddad, R. Houben, and W. Serdijn, "Analog wavelet transform employing dynamic translinear circuits for cardiac signal characterization," in *Proc. ISCAS*, 2003, vol. 1, pp. I-121–I-124.
[41] S. Haddad, J. Karel, R. Peeters, R. Westra, and W. Serdijn, "Analog complex wavelet filters," in *Proc. IEEE ISCAS*, 2005, vol. 4, pp. 3287–3290.
[42] S. Haddad, S. Bagga, and W. Serdijn, "Log-domain wavelet bases," *IEEE Trans. Circuits Syst. I, Reg. Papers*, vol. 52, no. 10, pp. 2023–2032, Oct. 2005.
[43] R. Edwards and M. Godfrey, "An analog wavelet transform chip," in *Proc. IEEE Int. Conf. Neural Netw.*, 1993, vol. 3, pp. 1247–1251.
[44] E. Justh and F. Kub, "Analogue CMOS high-frequency continuous wavelet transform circuit," *Electron. Lett.*, vol. 35, no. 1, pp. 4–5, Jan. 1999.
[45] R. Lyon and C. Mead, "An analog electronic cochlea," *IEEE Trans. Acoust., Speech, Signal Process.*, vol. 36, no. 7, pp. 1119–1134, Jul. 1988.
[46] L. Watts, D. Kerns, R. Lyon, and C. Mead, "Improved implementation of the silicon cochlea," *IEEE J. Solid-State Circuits*, vol. 27, no. 5, pp. 692–700, May 1992.
[47] W. Liu, M. Goldstein, and A. Andreou, "Multiresolution speech analysis with an analog cochlear model," in *Proc. IEEE-SP Int. Symp. Time-Freq. Time-Scale Anal.*, 1992, pp. 433–436.
[48] P. Furth and A. Andreou, "A design framework for low power analog filter banks," *IEEE Trans. Circuits Syst. I, Fundam. Theory Appl.*, vol. 42, no. 11, pp. 966–971, Nov. 1995.

Alfonso Chacón-Rodríguez (M'06) was born in San José, Costa Rica, in 1967. He received the B.S. degree in electronics engineering from the Instituto Tecnológico de Costa Rica, Cartago, Costa Rica, in 1990, the Magister Literarum in english literature from the University of Costa Rica, San Pedro, Costa Rica, in 2004, and the Ph.D. degree in engineering from the Universidad Nacional de Mar del Plata, Mar del Plata, Argentina, in 2009. Most of the work in this paper was developed while he was finishing his doctoral dissertation, working at the Instituto de Investigaciones en Ingeniería Eléctrica "Alfredo Desages," Universidad Nacional del Sur, Bahía Blanca, Argentina.

He is currently with the Escuela de Ingeniería Electrónica, Instituto Tecnológico de Costa Rica. His interests range from low-power analog and digital VLSIs, low-power signal processing, and digital systems architecture to Anglo-Indian and Latin American literature.

Pedro M. Julián (S'94–M'00–SM'05) received the Electronic Engineer and Ph.D. degrees in "control de sistemas" from the Universidad Nacional del Sur (UNS), Bahía Blanca, Argentina, in 1994 and 1999, respectively.

He was a Visiting Scholar at the University of California, Berkeley, in 2000–2002 and a Visiting Scholar (in 2002–2003) and a Visiting Fulbright Professor (in 2009) with Johns Hopkins University, Baltimore, MD. He is currently an Associate Professor with the Departamento de Ingeniería Eléctrica y de Computadoras, UNS, and an Independent Researcher with the National Research Council of Argentina (CONICET). He serves as an Associate Editor of the *International Journal of Circuit Theory and Applications*. His research interests include the theory and applications of computational circuits and systems, and electronic systems, particularly sensory processors (acoustic and vision), with emphasis on low-power VLSI systems.

Dr. Julián was the recipient of the Houssay 2009 Prize from the National Ministry of Science and Technology of the Argentina Republic. He also serves as an Associate Editor of the IEEE Circuits and Systems Society (CASS) Magazine and the CASS Newsletter. He served as the Region 9 (Latin America) Vice President and on the Board of Governors of the IEEE CASS from 2004 to 2007. He is a founding member of the Latin American Consortium for Integrated Services and the Argentine School of Microelectronics (EAMTA).

Liliana Castro received the B.S. and M.S. degrees in mathematics and the Ph.D. degree in control systems from the Universidad Nacional del Sur (UNS), Bahía Blanca, Argentina.

Since 2007, she has been a full Professor with the Departamento de Matemática, UNS, and she is also with the Instituto de Investigaciones en Ingeniería Eléctrica, UNS-CONICET. Since 2000, she has been the Head of the Modeling Group, Laboratorio de Investigación y Desarrollo en Visualización y Computación Gráfica, Departamento de Ciencias e Ingeniería de la Computación, UNS. Her research interests include nonlinear system modeling, identification, piecewise linear approximation of nonlinear systems, and geometric modeling using wavelets.

Pablo Alvarado (M'98) was born in Costa Rica in 1969. He received the B.Sc. degree in electronics from the Costa Rica Institute of Technology, Cartago, Costa Rica, in 1991 and the M.Sc. and Ph.D. degrees in computer engineering from the RWTH Aachen University, Aachen, Germany, in 1998 and 2004, respectively.

Since 2004, he has been an Associate Professor with the Escuela de Ingeniería Electrónica, Instituto Tecnológico de Costa Rica, Cartago. His interests include digital signal and image processing, computer vision, pattern recognition, and wireless sensor networks.

Néstor Hernández was born in Costa Rica in 1952. He received the B.S. degree in electric engineering from the University of Costa Rica, San Pedro, Costa Rica, in 1973 and the M.Sc. degree in electrical engineering from the Center of Research and Advanced Studies, National Polytechnic Institute of México, Mexico City, Mexico, in 1993. He is currently working toward the Ph.D. degree in forest fire early detection systems, using image processing, at the Escuela de Ingeniería Electrónica, Instituto Tecnológico de Costa Rica, Cartago, Costa Rica.

His interests include electromagnetic compatibility, radio and optical communication, and wireless sensor networks.